

A hierarchy of coexistence patterns mediating between low- and high-dimensional dynamics in highly symmetric systems

Sindre W. Haugland and Katharina Krischer^{a)}

Physics Department, Nonequilibrium Chemical Physics, Technical University of Munich, James-Frank-Str. 1, D-85748 Garching, Germany

(Dated: 17 March 2022)

Coupled oscillators, even identical ones, display a wide range of behaviours, among them synchrony and incoherence. The 2002 discovery of so-called chimera states, states of coexisting synchronized and unsynchronized oscillators, provided a possible link between the two and definitely showed that different parts of the same ensemble can sustain qualitatively different forms of motion. Here, we demonstrate that globally coupled identical oscillators can express a range of coexistence patterns more comprehensive than chimeras. A hierarchy of such states evolves from the fully synchronized solution in a series of cluster-splittings. At the far end of this hierarchy, the states further collide with their own mirror-images in phase space – rendering the motion chaotic, destroying some of the clusters and thereby producing even more intricate coexistence patterns. A sequence of such attractor collisions can ultimately lead to full incoherence of only single asynchronous oscillators. Chimera states, with one large synchronized cluster and else only single oscillators, are found to be just one step in this transition from low- to high-dimensional dynamics.

One of the big problems in physics is how high-dimensional disorder in space and time may emerge from a spatially ordered, in the simplest case uniform, state with low-dimensional dynamics¹. Exploring different paths from order to spatiotemporal disorder and their universal character is central for a deeper understanding of complex emergent behaviour such as spatiotemporal chaos in reaction-diffusion systems^{2,3} or turbulence in hydrodynamic flows^{4,5}.

Ensembles of coupled oscillators are one class of apparently simple dynamical systems that yet may adopt states ranging from full synchrony to complete incoherence, and which has provided insights in virtually any discipline, ranging from the natural sciences to sociology^{6,7}. During the last two decades, a kind of hybrid phenomenon, in which synchronized and incoherent oscillators coexist in an ensemble of identical oscillators⁸, coined a chimera state⁹, has received considerable attention (see Reviews^{10–12} and the references therein), not least since it can be considered a “natural link between coherence and incoherence”¹³. In an earlier study employing globally coupled logistic maps¹⁴, four different classes of behaviour were found, including a large variety of partially ordered states, some of which were later classified as chimeras¹⁵. Yet, the bifurcation structure between the different classes was not resolved.

In this article, we study the bifurcations from synchrony, via clustered and partially clustered states to full incoherence in a system of globally coupled oscillators with nonlinear coupling, with simulations and bifurcation analysis for an increasing number of oscillators. Here, chimera states are just one of a multitude of coexistence patterns, all consisting of clusters, that is, internally synchronized groups of oscillators, of widely

different sizes and dynamics, and possibly including one or several single oscillators. The path towards complete incoherence begins with a symmetry-breaking cascade of cluster-splitting period-doubling bifurcations, wherein the currently smallest cluster is repeatedly split into two, leading to hierarchical clustering. Due to the high symmetry of the system, each symmetry-breaking produces many equivalent mirror-image variants of each outcome state, multiplying the number of attractors and leading to an ever more crowded phase space¹⁶. At some point, each variant collides with some of its mirror-images, creating larger attractors with higher symmetry. Usually, this blows up some of the clusters, the resulting single oscillators henceforth moving similarly on average. A succession of such symmetry-increasing bifurcations destroys first the smallest clusters, and then the larger ones, partially mirroring the former cluster-splitting cascade and ultimately creating a completely incoherent state. A chimera state, consisting of one synchronized cluster and otherwise only single, incoherent oscillators is often the second to last state of the sequence.

The model we employ is an ensemble of N Stuart-Landau oscillators $W_k \in \mathbb{C}$, $k = 1, \dots, N$, with nonlinear global coupling¹⁷:

$$\frac{dW_k}{dt} = W_k - (1 + ic_2)|W_k|^2 W_k - (1 + i\nu)\langle W \rangle + (1 + ic_2)\langle |W|^2 W \rangle, \quad (1)$$

where c_2 and ν are real parameters and $\langle \dots \rangle = 1/N \sum_{k=1}^N \dots$ denotes ensemble averages. The Stuart-Landau oscillator itself is a generic model for a system close to a Hopf bifurcation, that is, to the onset of self-sustained oscillations¹⁸. Networks of such oscillators have previously been found to exhibit a wide range of dynamics, many of them occurring for linear global coupling^{19–23}. The nonlinear global coupling in equation (1) stands out by featuring two qualitatively different

^{a)}Electronic mail: krischer@tum.de.

chimera states, each of them deduced to somehow emerge from a corresponding type of two-cluster solution²⁴. Because the oscillators are identical and the coupling is global, the system is \mathbb{S}_N -equivariant: If $\mathbf{W}(t) \in \mathbb{C}^N$ is a solution, then so is $\gamma\mathbf{W}(t) \forall \gamma \in \mathbb{S}_N$, where \mathbb{S}_N is the *symmetric group* of all permutations of the N oscillators²⁵. Further, the average $\langle W \rangle$ is confined to simple harmonic motion with frequency ν , as shown by taking the ensemble average of the whole equation:

$$\left\langle \frac{dW_k}{dt} \right\rangle = \frac{d}{dt} \langle W \rangle = -i\nu \langle W \rangle \Rightarrow \langle W \rangle = \eta e^{-i\nu t}, \quad (2)$$

where $\eta \in \mathbb{R}$ is an additional parameter, implicitly set by choosing the initial condition. This constraint also implies that for a Poincaré map²⁶ defined by sampling the system with frequency ν , the average of the N components of the map will always be constant. Thus the nonlinear constraint in the time-continuous equation (1) becomes a linear constraint in the time-discrete map.

The fully synchronized solution $W_k = \eta e^{-i\nu t} \forall k$ always exists and is stable for sufficiently large values of η . It loses stability in either an equivariant pitchfork bifurcation, producing separate clusters that continue to orbit the origin with frequency ν at different fixed amplitudes, or an equivariant Hopf bifurcation to a T^2 torus, producing separate modulated-amplitude clusters that henceforth oscillate with two superposed frequencies ν and ω_H ²⁷. We will focus on the latter and the dynamics arising from these.

The Hopf bifurcation occurs at $\eta_H = 1/\sqrt{2}$ for suitable values of c_2 and ν . For $\nu = 0.1$, which we keep fixed throughout, it does for $c_2 < -0.448$ ¹⁷. At η_H , several differently balanced two-cluster solutions emerge from the synchronized solution, some as stable and some as unstable, depending on the value of c_2 . The balanced $N/2-N/2$ solution, with an equal number of oscillators in each cluster, is shown in Fig. 1 a. The dashed circle marks the enforced path of the ensemble average $\langle W \rangle = \eta e^{-i\nu t}$, which the two clusters orbit on opposite sides as it circles the origin.

Because $\langle W \rangle$ is independent of the individual oscillator dynamics, the value of any oscillator in the frame of reference of the ensemble average is always given by the simple transformation

$$W_k = \eta e^{-i\nu t} (1 + w_k) \Rightarrow w_k = W_k \eta^{-1} e^{i\nu t} - 1, \quad (3)$$

where w_k is the value of W_k in the co-rotating frame. There, the $N/2-N/2$ solution from Fig. 1 a is simply periodic with frequency ω_H and looks as in Fig. 1 b. An unbalanced modulated-amplitude cluster solution with cluster sizes $N_1 = 3N/4$ and $N_2 = N/4$ appears as in Fig. 1 c. The average of all oscillators in the co-rotating frame of $\langle W \rangle$ is of course always zero. Notably, the global coupling ensures that all solutions for an ensemble size N are also solutions for $N' = nN$, $n \in \mathbb{N}$, with every cluster scaled up by a factor of n . For solutions that contain only clusters $N_i \geq 2$, the stability properties will also be the same for different n ^{22,28}.

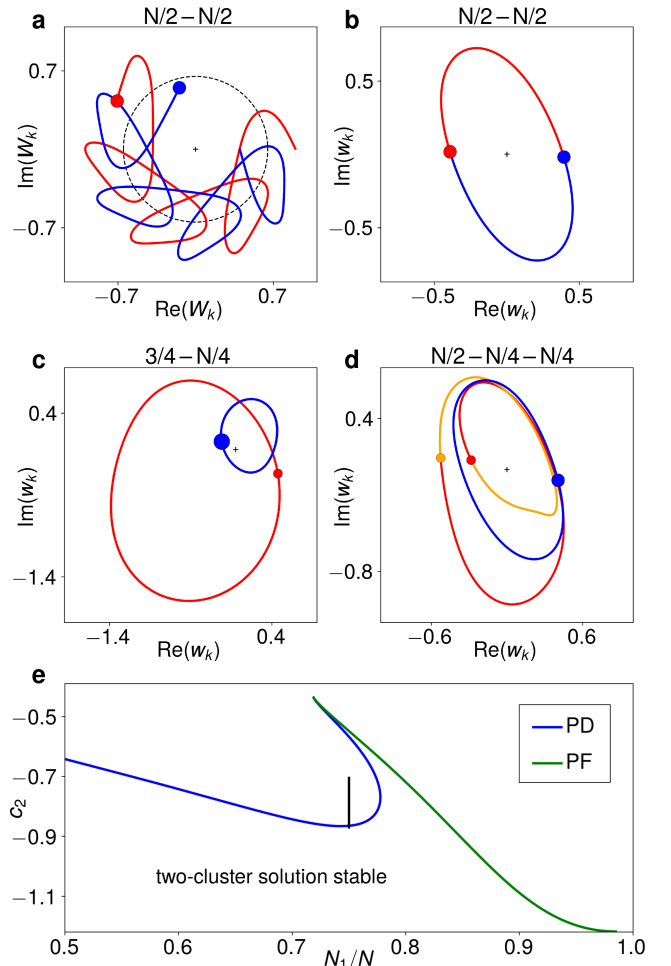


FIG. 1. **Two-cluster solutions and their bifurcations.** **a**, Trajectory of an $N/2 - N/2$ modulated-amplitude cluster solution for $c_2 = -0.71$ and $\eta = 0.65$. **b**, The solution in **a** when viewed in a frame co-rotating with the ensemble average $\langle W \rangle = \eta e^{-i\nu t}$. Here, the two clusters follow the same trajectory. **c**, Unbalanced $3N/4 - N/4$ two-cluster solution in the rotating frame at $c_2 = -1.0$ and $\eta = 0.65$. **d**, $N/2 - N/4 - N/4$ three-cluster solution at $c_2 = -0.69$, emerging from the solution in **a, b** in a period-doubling bifurcation. **e**, Bifurcations destabilizing the two-cluster solution as a function of c_2 and the relative size of the larger cluster N_1/N for $\eta = 0.67$. The blue line denotes a period-doubling (PD) that splits the smaller cluster and the green line a sub-critical pitchfork (PF) that blows it up. The vertical black line marks the c_2 -incremented simulation in Fig. 5.

If we start at a point in parameter space where the $N/2 - N/2$ solution is stable, keep $\eta < \eta_H$ sufficiently close to the Hopf bifurcation and gradually increase c_2 , one of the two clusters will break up into two smaller clusters. A possible outcome is shown in Fig. 1 d. The trajectory of the two new clusters is no longer simply periodic, but period-2, with a small and a large loop. The $N/2 - N/2$ solution has thus become unstable in a symmetry-breaking period-doubling bifurcation, giving rise to a stable $N/2 - N/4 - N/4$ three-cluster so-

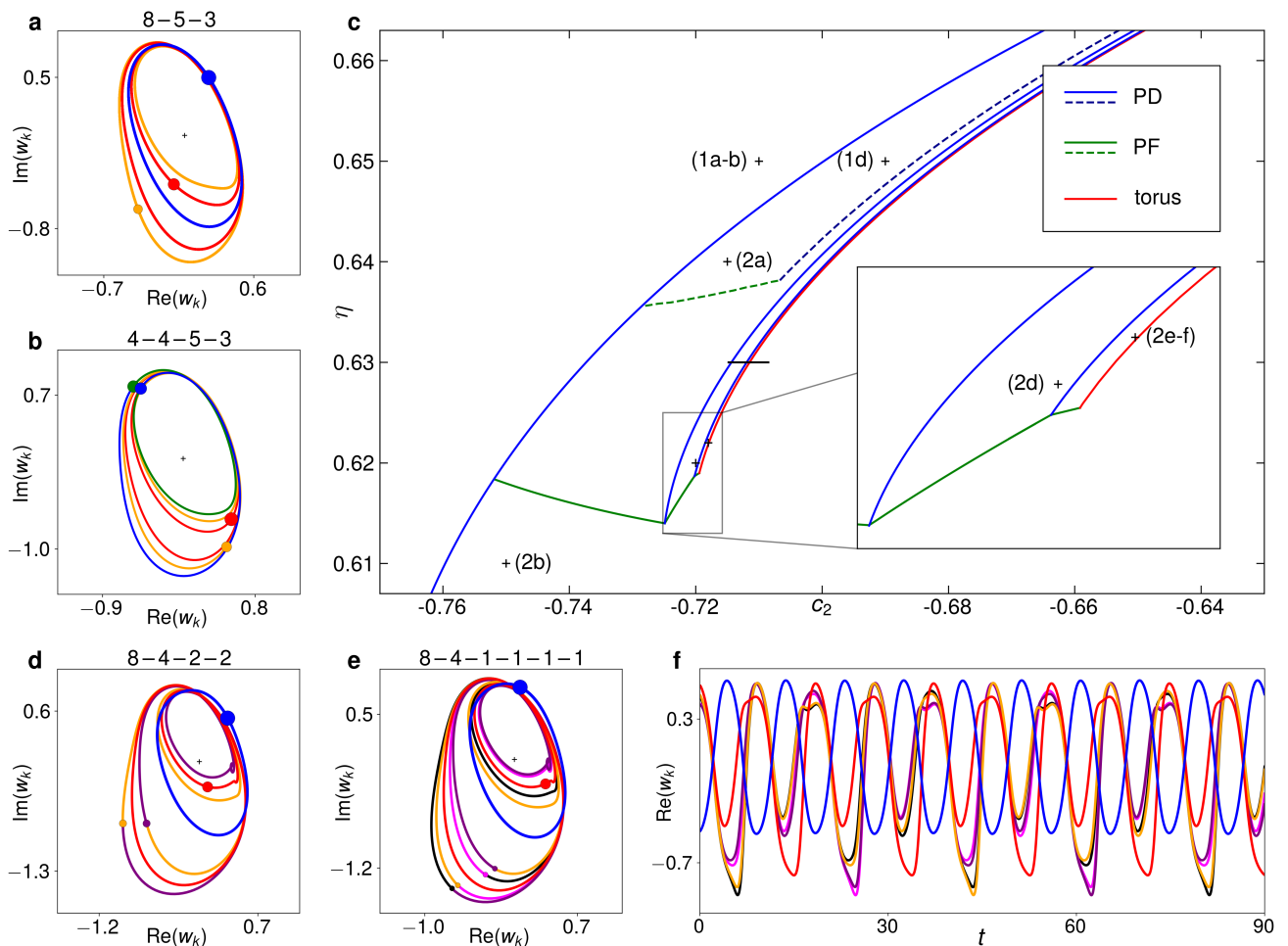


FIG. 2. **Cluster solutions and bifurcations for $N = 16$.** Sizes of filled circles mirror sizes of clusters. **a**, 8-5-3 solution in the co-rotating frame of $\langle W \rangle$ for $c_2 = -0.715$ and $\eta = 0.64$. **b**, 4-4-5-3 solution for $c_2 = -0.75$ and $\eta = 0.61$. **c**, Bifurcation diagram of 8-8-derived solutions with PD=period-doubling, PF=pitchfork. Dashed lines mark bifurcations of the 8-5-3 solution (a), solid lines those of the 8-4-4 (Fig. 1d) and the solutions emerging from it. Labeled crosses mark parameter values of depicted complex-plane portraits. The black line marks the c_2 -incremented simulation in Fig. 3 a,b. **d**, 8-4-2-2 solution for $c_2 = -0.72$ and $\eta = 0.62$. **e,f**, 8-4-1-1-1-1-1 solution for $c_2 = -0.718$ and $\eta = 0.62$, including time series of real part of each cluster and single oscillator.

lution. This bifurcation also destabilizes less balanced two-cluster solutions, for which the smaller of the two clusters is split. Its position in parameter space depends on the relative sizes of the clusters, as shown in Fig. 1 e. For very unbalanced solutions, the smallest cluster is explosively destroyed in a subcritical pitchfork bifurcation.

HIERARCHICAL CLUSTERING THROUGH PERVASIVE STEPWISE SYMMETRY BREAKING

The first period-doubling bifurcation curve is followed by a mesh of additional cluster-splitting bifurcations curves, creating a hierarchy of successively less symmetric multi-cluster solutions with various periodicities. Each bifurcation involves the breakup of either one cluster or two similarly behaving clusters and produces several

qualitatively different solutions, differing by how the oscillators of the splitting cluster(s) distribute. (For example, the 4-4 solution for $N = 8$ can split into either 4-2-2, 4-3-1, 2-2-2-2, 2-2-3-1 or 3-1-3-1.) However, all these solutions will usually not be co-stable.

Fig. 2 c shows the stability boundaries of several solutions for $N = 16$. The 8-8 solution is stable in the upper left. When increasing c_2 for $\eta > 0.635$, it gives rise to stable 8-4-4 and 8-5-3 solutions (Figs. 1 d and 2 a, respectively) at the leftmost blue period-doubling line. The 8-5-3 solution is stable within the two dashed lines. Below the dashed green line, it in turn produces a stable 5-3-5-3 and unstable 5-3-6-2 and 5-3-7-1 solutions. At the dashed blue line, the 8-5-3 solution undergoes another period-doubling cluster split to an 8-5-2-1 period-4 solution.

The solid lines all affect the 8-4-4 solution and its

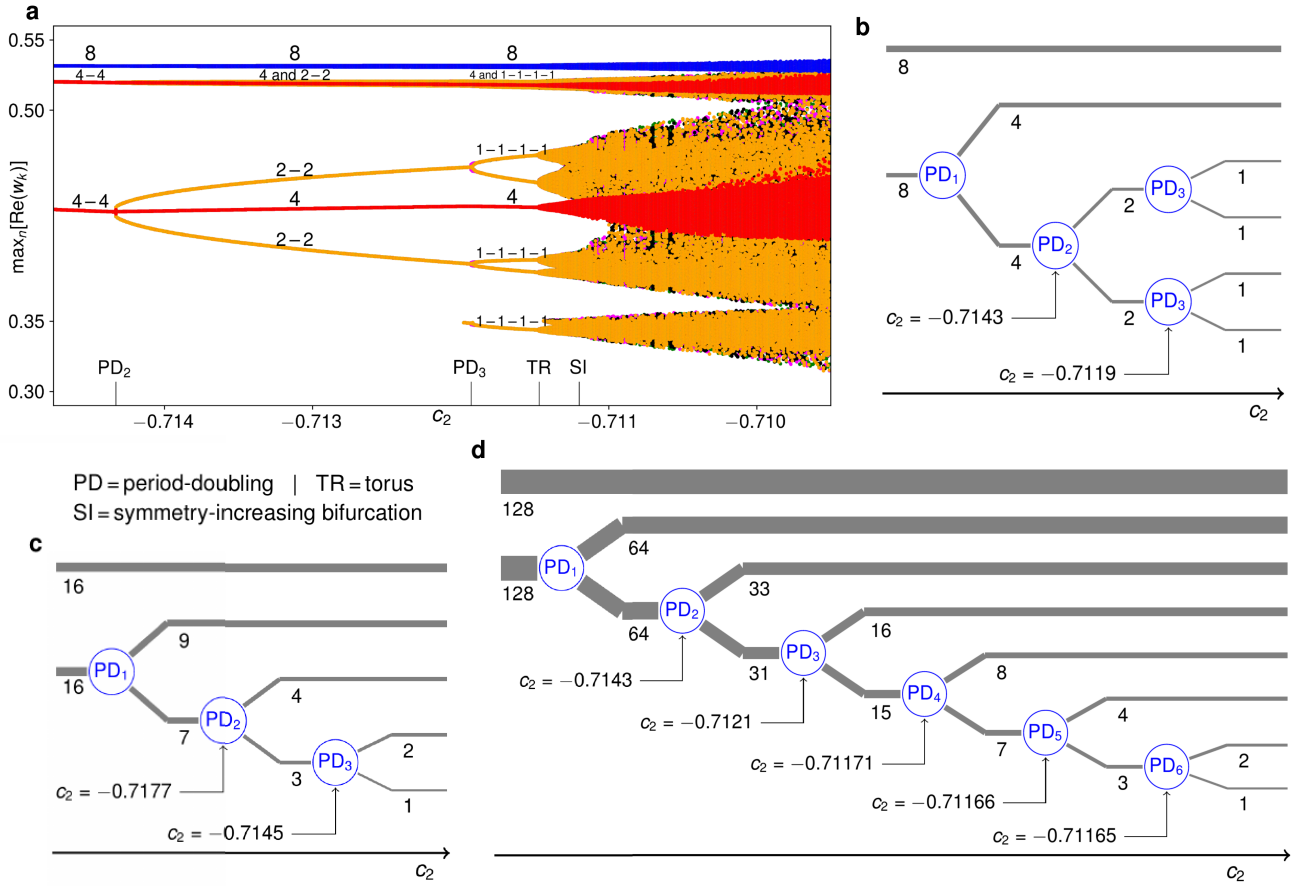


FIG. 3. **Cluster-splitting cascades for different N .** **a**, Maxima of $\operatorname{Re}(w_k)$ in an $N = 16$ c_2 -incremented simulation at $\eta = 0.63$. Labels on the figure mark the clusters reaching the different maxima as the solution changes from $8-4-4$ via $8-4-2-2$ to $8-4-(4 \times 1)$. Labels on the abscissa mark occurring bifurcations. The additional smallest yellow maximum appearing at $c_2 \approx -0.712$ is caused by the continuous deformation of the oscillator trajectories and not by a bifurcation. At $c_2 \approx -0.7115$, the torus bifurcation to three-frequency dynamics manifests itself in a distinct broadening of the formerly discrete maxima. **b**, Schematic portrayal of the period-doubling cluster splittings in the simulation in **a**. **c,d**, Like **b** for c_2 -incremented simulations at $\eta = 0.63$ with $N = 32$ and $N = 256$, respectively, based on quantitative results in Supplementary Figures 1-3.

descendants. At the solid green line from $c_2 \approx -0.755$ to $c_2 \approx -0.725$ in the lower left, it produces stable $4-4-4-4$ and $4-4-5-3$ (Fig. 2 b) solutions, as well as unstable $4-4-6-2$ and $4-4-7-1$ solutions. Like the dashed green line, this is an equivariant pitchfork bifurcation, splitting clusters, but not altering the overall periodicity of the ensemble. Below these lines, the above-mentioned four-cluster solutions also emerge directly from the $8-8$ solution at the leftmost period-doubling line.

At the solid blue line directly to the right of the dashed blue one, the $8-4-4$ solution undergoes a period-doubling bifurcation analogous to that of the $8-5-3$ solution, producing a stable $8-4-2-2$ (Fig. 2 d) and an unstable $8-4-3-1$ period-4 solution. The former becomes unstable at the bottom diagonal green pitchfork line at $c_2 \approx -0.72$, where it produces a stable $4-4-4-2-2$ solution. This solution also emerges directly from the $4-4-4-4$ solution in a period-doubling bifurcation not shown.

At the rightmost blue period-doubling line (see inset), the $8-4-2-2$ solution produces an unstable $8-4-2-1-1$

and a stable $8-4-1-1-1-1$ period-8 solution (Fig. 2e-f). At the red line in Fig. 2 c, the $8-4-1-1-1-1-1$ solution undergoes a torus bifurcation, whereby a third frequency is added to the dynamics, while all clusters stay intact. The resultant three-frequency motion is resistant to the addition of small random numbers over a nonzero c_2 interval, which is notable in light of a prior proof that quasiperiodic dynamics with three or more frequencies are in general structurally unstable^{1,29}. Such stable quasi-periodic motion on T^3 has also been observed in Stuart-Landau oscillators with linear global coupling²⁰ and could be caused by the rotational invariance of the differential equations.

If we initialize the $8-4-4$ solution at $c_2 = -0.71$ and $\eta = 0.63$ and slowly increase c_2 along the horizontal black line in Fig. 2 c, the maxima of $\operatorname{Re}(w_k)$ for $k = 1, \dots, 16$ develop as in Fig. 3 a: Initially, there are one maximum of the oscillators in the cluster of eight (blue) and two shared maxima of the two clusters of four (red). When one of these clusters splits up into two clusters of two at

PD₂, their maxima appear as four distinct yellow lines. In the next period-doubling cluster split, these lines split up into eight.

From the fully synchronized solution to the 8–4–(4×1) solution, four discrete steps of symmetry breaking have taken place. The three last of these steps are shown schematically in Fig. 3 b. Similar stepwise symmetry-breaking is observed both for larger N and when the smallest cluster does not break up into equal-sized parts (Fig. 3 c). The larger N is, the more steps occur, at ever closer parameter values, and for $N = 256$, as many as seven steps can be observed (see Fig. 3 d). The two-cluster solutions thus give rise to a cluster-splitting cascade, producing a multitude of coexisting multi-cluster states and, most notably, hierarchical clustering.

SYMMETRY-INCREASING BIFURCATION AND PRECISION-DEPENDENT CLUSTERING

At the end of a cascade of cluster-splitting period-doubling bifurcations, a torus bifurcation usually occurs. The resultant T^3 motion is usually stable for a nonzero parameter interval, before being superseded by less regular dynamics in a *symmetry-increasing bifurcation*³⁰. Because equation (1) is \mathbb{S}_N -equivariant, any solution remains a solution when any of the oscillators are interchanged, and each solution (except the fully synchronized one) exists in the form of several distinct symmetric variants in phase space. (For example, if we interchanged an oscillator from the blue cluster in Fig. 1 a with one from the red, the outcome would be such a different, but equivalent variant.)

If two or more variants grow to touch each other, they merge to become a single instance of a new solution, of which there are fewer distinct mirror-image variants in total. The attractor on which the new solution lives is correspondingly more symmetric than the attractors of the colliding variants. One symmetry-increasing bifurcation can in general be followed by another, further increasing the attractor symmetry. In the $N = 16$ case in Fig. 3 a, the first symmetry-increasing bifurcation only disrupts the former cyclic order of the four single oscillators, inherited from the solution in Fig. 2 e-f (i.e., that the purple oscillator trails the yellow one, which trails the pink, and so on). In other cases, some of the intact clusters of a colliding variant contain oscillators that are in a different cluster in some of the other colliding variants. Then, the symmetry-increasing bifurcation destroys these clusters. (Because the colliding variants have identical properties, they must namely all be treated equally by the collision, and if two oscillators that are clustered in only some of these variants were to remain permanently together, this would not be the case.) Hence, as the attractor symmetry is increased, the number of single oscillators, in general, grows, in a sense also decreasing the overall order of the ensemble.

Past the $N = 32$ cluster-splitting cascade in Fig. 3 c,

the long-term cluster-size distribution at some point becomes 16–9–(7×1). A time series of the resulting solution is shown in Fig. 4 a: Here, the seven single oscillators in yellow move similarly to the clusters of four, two and one in the former 16–9–4–2–1 solution, being close to deep minima when the red cluster of nine is at a shallow minimum and vice versa. They also repeatedly congregate into temporary agglomerations of four, three and two oscillators, respectively, as illustrated in Fig. 4 b-d. Here, the cross-correlation between all oscillator trajectories is calculated every 10^4 time steps. Two oscillators are said to be in the same cluster if their cross-correlation

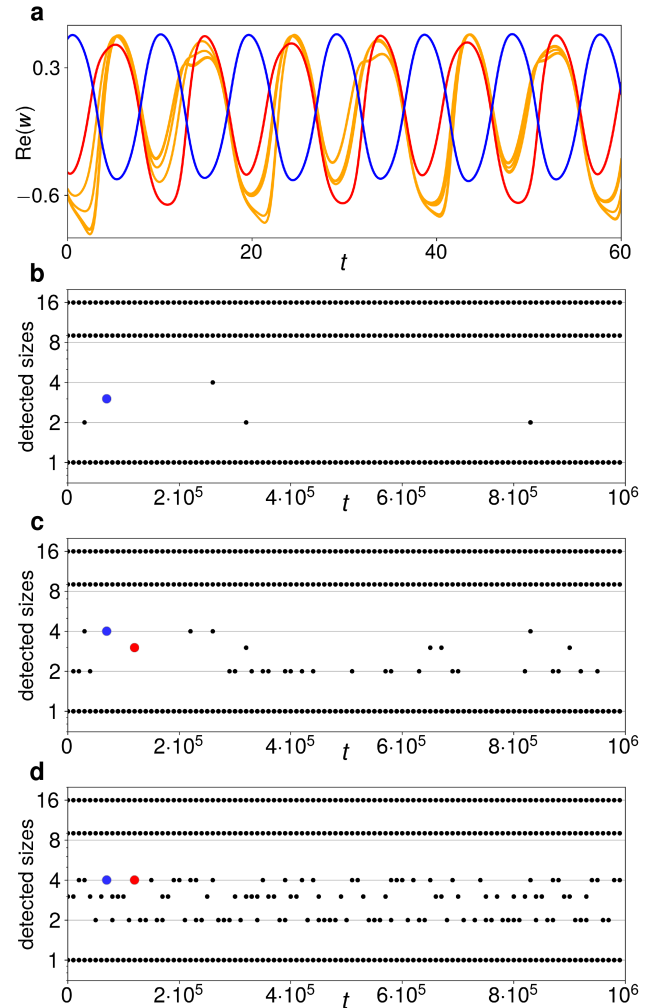


FIG. 4. **Partially clustered 16–9–(7×1) solution past the cascade in Fig. 3 c.** **a**, Time series of $\text{Re}(w_k)$ for $c_2 = -0.712$ and $\eta = 0.63$. The single oscillators (yellow) reach a deep minimum approximately when the cluster of nine (red) reaches a shallow minimum and the cluster of 16 a maximum. **b-d**, Clusters sizes detected when two oscillators are said to be clustered if their cross-correlation over an interval of 800 time units is $> 1 - \varepsilon$ for $\varepsilon = 10^{-8}$, 10^{-4} and 10^{-2} , respectively. The large red and blue dots mark two exemplary loose oscillator conglomerations at different sensitivities ε .

is greater than $1 - \varepsilon$ for $\varepsilon = 10^{-8}$ (b), $\varepsilon = 10^{-4}$ (c) or $\varepsilon = 10^{-2}$ (d). Sometimes, a temporary cluster of three becomes a cluster of four for larger values of ε , such as the blue cluster at $t = 7 \cdot 10^4$ and the red cluster at $t = 1.2 \cdot 10^5$. This probably marks less close approaches to the 16–9–4–2–1 remains, when three out of four congregating oscillators are more correlated than the fourth.

If c_2 is sufficiently increased, the ensemble will often jump to an entirely different solution, and beyond the state in Fig. 4, it jumps to the 16–8–8-derived branch. However, the end result can also be the destruction of all permanent clusters and the motion of only single oscillators on a fully symmetric chaotic attractor. See Supplementary Figures 4–6.

Dynamics like those in Fig. 4 have previously been observed in globally coupled logistic maps when phase space becomes so full of mirror-image attractors that they inevitably intrude upon each other³¹. The outcome is a form of *chaotic itinerancy*³², wherein the system meanders between the *attractor ruins* of previous attractors, each of them relatively low-dimensional, but connected by higher-dimensional transitional motion¹⁵.

Also found in globally coupled maps is *precision-dependent clustering*, wherein maps that are unclustered when distinguished with high precision appear to repeatedly merge into the ever thicker branches of a clustering tree when the precision is decreased¹⁴. In our ensemble, this occurs as a consequence of the symmetry-breaking period-doubling cascade. For example, past the $N = 256$ cascade in Fig. 3 (at $c_2 \approx -0.71162$), we encounter a 128–64–33–(31×1) itinerant solution that for small $\varepsilon \leq 10^{-5}$ is found to have an additional cluster of usually 16, sometimes 18 or 19 oscillators, while the remaining oscillators repeatedly form ephemeral smaller clusters of strongly fluctuating sizes. For $\varepsilon = 10^{-4}$, a cluster of size 15 is also sometimes detected, and for $\varepsilon = 10^{-3}$ the sizes are always 128–64–33–16–15, 128–64–33–18–13 or 128–64–33–19–12. For $\varepsilon = 10^{-2}$, they are 128–33–31 throughout, and for $\varepsilon = 10^{-1}$, 128–64–64. The same pattern to some extent already applies in the quasiperiodic domain of Fig. 3 b–d, where clusters are most strongly correlated with those other clusters from which they most recently split.

EMERGENCE OF A CHIMERA STATE

In our context, a chimera state is a $N_1 - ((N - N_1) \times 1)$ solution. The modulated-amplitude chimeras previously found in equation (1) have significantly more synchronized (N_1) than unsynchronized ($N - N_1$) oscillators³³. This suggests they have not evolved from balanced two-cluster solutions. Yet, our above results can be used to explain how they are created. If we e.g. initialize an $N = 20$ ensemble as a 15–5 solution (Fig. 5 a) for $c_2 = -0.87$ and $\eta = 0.67$, Fig. 1 e tells us it will undergo a cluster-splitting period-doubling bifurcation if c_2 is increased. The resulting 15–3–2 period-2 solution is shown

in Fig. 5 b. Further up in c_2 , the cluster of two is split into single oscillators (Fig. 5 c). Then, a torus bifurcation smears the previously closed trajectories into continuous bands (Fig. 5 d).

Finally, the current 15–3–1–1 variant collides with nine others in a symmetry-increasing bifurcation. This destroys the cluster of three, resulting in a 15–(5×1) chimera state (Fig. 5 e). Note how the three oscillators that are temporarily close to each other in Fig. 5 e (red, yellow, grey, in the lower left) are not all the same three that were clustered in Figs. 5 b–d (red, purple, grey). The ensemble is currently close to the ruin of a different 15–3–1–1 solution variant, and the chimera state is thus also an example of chaotic itinerancy. For $N = 200$, the transition from a 150–50 to a 150–(50×1) solution proceeds along a much more involved, but essentially similar path. See Supplementary Figure 7.

CONCLUDING REMARKS

Above, we have shown how a system of identical units successively splits up into ever more complex coexistence patterns. The high symmetry of the equations is probably central to the bifurcation scenario observed, as \mathbb{S}_N not only has many subgroups, but most of these subgroups have many subgroups as well, and so on. This intricate subgroup structure is mirrored in the hierarchy of successively less symmetric quasiperiodic solutions. Moreover, because \mathbb{S}_N is much larger than those of its subgroups corresponding to the more intricate solutions, there are many mirror-image variants of the latter, causing the symmetry-increasing bifurcations and the itinerant coexistence patterns that these produce.

In globally coupled maps, multi-cluster states, precision-dependent clustering, chimeras and chaotic itinerancy have all been previously reported, but without an overall explanation of how they are bifurcation-theoretically created and connected to each other^{14,15}. This suggests that the bifurcation scenario uncovered here is universal to \mathbb{S}_N -equivariant ensembles and possibly to other highly symmetric systems.

To trigger the observed symmetry-increasing bifurcation, it seems as if a certain dimensionality of the dynamics is needed. In our system, this is provided by the torus bifurcations, in the globally coupled maps by a period-doubling cascade to chaos. For Stuart-Landau oscillators with linear global coupling, a symmetry-increasing bifurcation has also been found to succeed a period-doubling cascade in an $N = 4$ system³⁴. To test whether hierarchical clustering and symmetry-increasing events mediate between synchrony and incoherence there as well, is an exciting task for future studies.

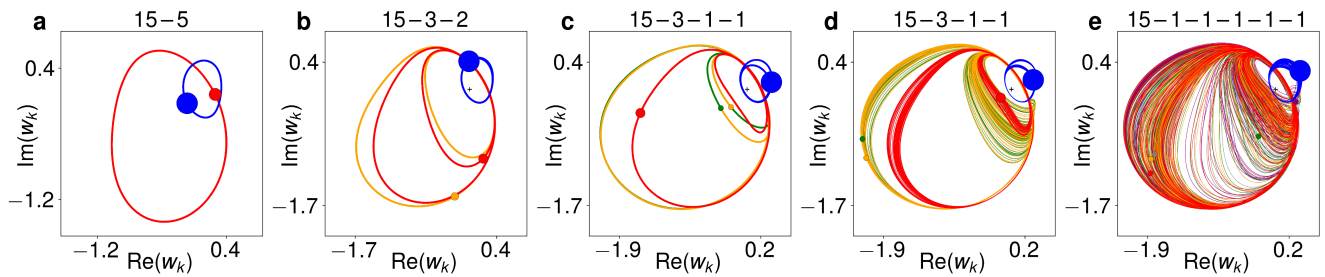


FIG. 5. **Steps from 15–5 two-cluster solution to chimera state.** $N = 20$, $\nu = 0.1$ and $\eta = 0.67$, proceeding along the black line in Fig. 1 e. **a**, 15–5 solution for $c_2 = -0.87$. **b**, 15–3–2 period-2 solution for $c_2 = -0.82$. **c**, 15–3–1–1 period-4 solution for $c_2 = -0.725$. The two largest loops of the two single oscillators are almost equal. **d**, 15–3–1–1 three-frequency solution for $c_2 = -0.71$. **e**, 15–(5 \times 1) chimera at $c_2 = -0.705$, after collision of mirror-image attractors.

REFERENCES

- ¹Argyris, J. H., Faust, G., Haase, M. & Friedrich, R. *An Exploration of Dynamical Systems and Chaos* (Springer Berlin Heidelberg, Berlin, Heidelberg, 2015).
- ²Cross, M. C. & Hohenberg, P. C. Pattern formation outside of equilibrium. *Rev. Mod. Phys.* **65**, 851–1112 (1993).
- ³Cross, M. C. & Hohenberg, P. C. Spatiotemporal Chaos. *Science* **263**, 1569–1570 (1994).
- ⁴Nelkin, M. In What Sense Is Turbulence an Unsolved Problem? *Science* **255**, 566–570 (1992).
- ⁵Warhaft, Z. Turbulence in nature and in the laboratory. *Proc. Natl. Acad. Sci.* **99**, 2481–2486 (2002).
- ⁶Strogatz, S. H. From Kuramoto to Crawford: Exploring the onset of synchronization in populations of coupled oscillators. *Phys. D Nonlinear Phenom.* **143**, 1–20 (2000).
- ⁷Pikovsky, A., Rosenblum, M. & Kurths, J. *Synchronization*. Cambridge Nonlinear Science Series (Cambridge Univ. Press, Cambridge, 2001).
- ⁸Kuramoto, Y. & Battogtokh, D. Coexistence of Coherence and Incoherence in Nonlocally Coupled Phase Oscillators. *Nonlinear Phenom. Complex Syst.* **5**, 380–385 (2002).
- ⁹Abrams, D. M. & Strogatz, S. H. Chimera states for coupled oscillators. *Phys. Rev. Lett.* **93**, 174102 (2004).
- ¹⁰Panaggio, M. J. & Abrams, D. M. Chimera states: Coexistence of coherence and incoherence in networks of coupled oscillators. *Nonlinearity* **28**, R67–R87 (2015).
- ¹¹Schöll, E. Synchronization patterns and chimera states in complex networks: Interplay of topology and dynamics. *Eur. Phys. J. Spec. Top.* **225**, 891–919 (2016).
- ¹²Omel’chenko, O. E. The mathematics behind chimera states. *Nonlinearity* **31**, R121–R164 (2018).
- ¹³Omel’chenko, O. E., Maistrenko, Y. L. & Tass, P. A. Chimera states: The natural link between coherence and incoherence. *Phys. Rev. Lett.* **100**, 044105 (2008).
- ¹⁴Kaneko, K. Clustering, coding, switching, hierarchical ordering, and control in a network of chaotic elements. *Phys. D Nonlinear Phenom.* **41**, 137–172 (1990).
- ¹⁵Kaneko, K. From globally coupled maps to complex-systems biology. *Chaos* **25**, 097608 (2015).
- ¹⁶Wiesenfeld, K. & Hadley, P. Attractor crowding in oscillator arrays. *Phys. Rev. Lett.* **62**, 1335–1338 (1989).
- ¹⁷Schmidt, L., Schönleber, K., Krischer, K. & García-Morales, V. Coexistence of synchrony and incoherence in oscillatory media under nonlinear global coupling. *Chaos* **24**, 013102 (2014).
- ¹⁸Kuramoto, Y. *Chemical Oscillations, Waves, and Turbulence*, vol. 19 of Springer Series in Synergetics (Springer Berlin Heidelberg, Berlin, Heidelberg, 1984).
- ¹⁹Hakim, V. & Rappel, W. J. Dynamics of the globally coupled complex Ginzburg-Landau equation. *Phys. Rev. A* **46**, R7347–R7350 (1992).
- ²⁰Nakagawa, N. & Kuramoto, Y. Collective Chaos in a Population of Globally Coupled Oscillators. *Prog. Theor. Phys.* **89**, 313–323 (1993).
- ²¹Sethia, G. C. & Sen, A. Chimera states: The existence criteria revisited. *Phys. Rev. Lett.* **112**, 144101 (2014).
- ²²Ku, W. L., Girvan, M. & Ott, E. Dynamical transitions in large systems of mean field-coupled Landau-Stuart oscillators: Extensive chaos and cluster states. *Chaos* **25**, 123122 (2015).
- ²³Kemeth, F. P., Haugland, S. W. & Krischer, K. Cluster singularity: The unfolding of clustering behavior in globally coupled Stuart-Landau oscillators. *Chaos* **29**, 023107 (2019).
- ²⁴Schmidt, L. & Krischer, K. Clustering as a prerequisite for chimera states in globally coupled systems. *Phys. Rev. Lett.* **114**, 034101 (2015).
- ²⁵Moehlis, J. & Knobloch, E. Equivariant dynamical systems. *Scholarpedia* **2**, 2510 (2007).
- ²⁶Strogatz, S. H. *Nonlinear Dynamics and Chaos: With Applications to Physics, Biology, Chemistry, and Engineering* (Routledge Taylor and Francis Group, Oxford, 1994).
- ²⁷Schmidt, L. & Krischer, K. Two-cluster solutions in an ensemble of generic limit-cycle oscillators with periodic self-forcing via the mean-field. *Phys. Rev. E* **90**, 042911 (2014).
- ²⁸Sorrentino, F., Pecora, L. M., Hagerstrom, A. M., Murphy, T. E. & Roy, R. Complete characterization of the stability of cluster synchronization in complex dynamical networks. *Sci. Adv.* **2**, 1–9 (2016).
- ²⁹Newhouse, S., Ruelle, D. & Takens, F. Occurrence of strange Axiom A attractors near quasi periodic flows on T^m , $m \geq 3$. *Commun. Math. Phys.* **64**, 35–40 (1978).
- ³⁰Chossat, P. & Golubitsky, M. Symmetry-increasing bifurcation of chaotic attractors. *Phys. D Nonlinear Phenom.* **32**, 423–436 (1988).
- ³¹Kaneko, K. Dominance of Milnor attractors in globally coupled dynamical systems with more than 7 ± 2 degrees of freedom. *Phys. Rev. E* **66**, 055201 (2002).
- ³²Kaneko, K. & Tsuda, I. Chaotic itinerancy. *Chaos* **13**, 926–936 (2003).
- ³³Schmidt, L. & Krischer, K. Chimeras in globally coupled oscillatory systems: From ensembles of oscillators to spatially continuous media. *Chaos* **25**, 64401 (2015).
- ³⁴Kemeth, F. P., Haugland, S. W. & Krischer, K. Symmetries of Chimera States. *Phys. Rev. Lett.* **120**, 214101 (2018).
- ³⁵Olivant, T. E. Python for scientific computing. *Comput. Sci. Eng.* **9**, 10–20 (2007).
- ³⁶Virtanen, P. et al. SciPy 1.0: fundamental algorithms for scientific computing in Python. *Nat. Methods* **17**, 261–272 (2020).
- ³⁷Van Der Walt, S., Colbert, S. C. & Varoquaux, G. The NumPy array: A structure for efficient numerical computation. *Comput. Sci. Eng.* **13**, 22–30 (2011).

³⁸Hunter, J. D. Matplotlib: A 2D graphics environment. *Comput. Sci. Eng.* **9**, 90–95 (2007).

³⁹Doedel, E. J. AUTO: A program for the automatic bifurcation analysis of autonomous systems. *Congr. Numer.* **30**, 265–284 (1981).

⁴⁰Doedel, E. & Oldeman, B. *Auto 07p: Continuation and bifurcation software for ordinary differential equations..* Tech. rep. (Concordia University and McGill HPC Centre, Montreal, 2019).

METHODS

The differential equations (1) were solved numerically using the Python programming language³⁵ (version 2.7 and later 3.8) and the implicit Adams method of the `scipy.integrate.ode` class of the SciPy library³⁶ (version 1.6) with a time step of $\Delta t = 0.01$. The data were held and processed in the form of NumPy (version 1.19) arrays³⁷ with complex-valued floating-point elements and visualized using the Matplotlib library and graphics environment (version 3.3)³⁸. The numerical results were evaluated using custom-built functions drawing on the resources of these standard Python libraries, written by S.W.H. Simulations were carried out in the non-rotating frame of equation (1), and results in the co-rotating frame of $\langle W \rangle$ were visualized applying equation (3) to the data *after* simulations had been carried out. When not otherwise stated, initial conditions of numerical solutions were random numbers on the real line, fulfilling the global constraint that $\langle W \rangle = \eta e^{-i\nu t}$. This choice was inspired by earlier work¹⁷.

Figs. 1e and 2c were created using the dynamical-systems continuation software Auto07p^{39,40} to continue solutions in parameter space. As Auto can only continue fixed-point and limit-cycle solutions, equation (1) had to be formulated in the co-rotating frame of the ensemble average in order to carry out these continuations, yielding

$$\begin{aligned} \frac{da_k}{dt} &= a_k - \nu b_k - \eta^2 [A_k - c_2 B_k] \\ &\quad + \frac{1}{N} \eta^2 \sum_j [A_j - c_2 B_j], \\ \frac{db_k}{dt} &= b_k + \nu a_k - \eta^2 [B_k + c_2 A_k] \\ &\quad + \frac{1}{N} \eta^2 \sum_j [B_j + c_2 A_j], \end{aligned} \quad (4)$$

where $w_k = a_k + ib_k$ with $a_k, b_k \in \mathbb{R}$, $k = 1, \dots, N$, and

$$\begin{aligned} A_k &= 3a_k + 3a_k^2 + a_k^3 + a_k b_k^2 + b_k^2, \\ B_k &= b_k + 2a_k b_k + a_k^2 b_k + b_k^3. \end{aligned} \quad (5)$$

To obtain Fig. 2c, the relevant $N = 16$ quasiperiodic solutions were first generated using Python simulations. The output data were transferred to the rotating frame, and a time series corresponding to one full period in that frame was used as input for a c_2 or η one-parameter continuation of each periodic solution, in order to detect the

location of the depicted bifurcations. Then, the detected bifurcations were two-parameter continued in c_2 and η to obtain the depicted bifurcation lines.

To obtain Fig. 1e, equation (4) was reduced to a two-cluster model by setting $a_k = a_{c1}$ and $b_k = b_{c1}$ for all $k = 1, \dots, N_1$, where $w_{c1} = a_{c1} + ib_{c1}$ is the value of the first cluster. All other oscillators $k = N_1 + 1, \dots, N$ are in the other cluster $w_{c2} = a_{c2} + ib_{c2}$. This yields the following equation for the first cluster

$$\begin{aligned} \frac{da_{c1}}{dt} &= a_{c1} - \nu b_{c1} \\ &\quad + \eta^2 \left(1 - \frac{N_1}{N}\right) [A_{c2} - A_{c1} - c_2 (B_{c2} - B_{c1})], \\ \frac{db_{c1}}{dt} &= b_{c1} + \nu a_{c1} \\ &\quad + \eta^2 \left(1 - \frac{N_1}{N}\right) [c_2 (A_{c2} - A_{c1}) + B_{c2} - B_{c1}], \end{aligned} \quad (6)$$

with A_{c1} and B_{c1} analogous to equation (5), while $w_{c2} = \frac{N_1}{N-N_1} w_{c1}$, because of the constraint that $\sum_k w_k = 0$. Thus, the reduced two-cluster model is only two-dimensional. The relative size of the first cluster, N_1/N , becomes an effective fourth parameter, in addition to c_2 , ν and η .

Whereas (6) describes the motion of two clusters of sizes N_1 and $N_2 = N - N_1$, respectively, it says nothing about intra-cluster stability and cannot model the breakup of either cluster. To be able to evaluate the internal stability of the clusters, we followed Ku et al.²² and added two effectively infinitesimal extra oscillators to the model, which only feel the presence of the two macroscopic clusters, but themselves neither affect the movement of each other, nor that of the macroscopic clusters. Their motion is given by

$$\begin{aligned} \frac{dp_{1,2}}{dt} &= p_{1,2} - \nu q_{1,2} - \eta^2 [P_{1,2} - c_2 Q_{1,2}] \\ &\quad + \eta^2 \left[\frac{N_1}{N} (A_{c1} - c_2 B_{c1}) \right. \\ &\quad \left. + \frac{N - N_1}{N} (A_{c2} - c_2 B_{c2}) \right], \\ \frac{dq_{1,2}}{dt} &= q_{1,2} + \nu p_{1,2} - \eta^2 [Q_{1,2} + c_2 P_{1,2}] \\ &\quad + \eta^2 \left[\frac{N_1}{N} (B_{c1} + c_2 A_{c1}) \right. \\ &\quad \left. + \frac{N - N_1}{N} (B_{c2} + c_2 A_{c2}) \right], \end{aligned} \quad (7)$$

where $P_{1,2}$ and $Q_{1,2}$ denote composite expressions for the first and second infinitesimal oscillator, of the same form

as A_{c_1, c_2} and B_{c_1, c_2} :

$$\begin{aligned} P_{1,2} &:= 3p_{1,2} + 3(p_{1,2})^2 + (p_{1,2})^3 \\ &\quad + p_{1,2}(q_{1,2})^2 + (q_{1,2})^2, \\ Q_{1,2} &:= q_{1,2} + 2p_{1,2}q_{1,2} + (p_{1,2})^2q_{1,2} + (q_{1,2})^3. \end{aligned} \quad (8)$$

In the initial state of the continuation, one of these two infinitesimal oscillators is set to follow the same periodic orbit as either of the two clusters. If any bifurcations are detected to make either infinitesimal oscillator leave the macroscopic cluster it started at, this means that cluster has become unstable.

Fig. 3a was created by initializing the $N = 16$ ensemble in the 8-4-4 configuration at $c_2 = -0.715$ and incrementing c_2 by $\Delta c_2 = 10^{-5}$ every $\Delta T = 4 \cdot 10^4$ time steps until $c_2 = -0.7095$ for $\nu = 0.1$ and $\eta = 0.63$. At the beginning of each c_2 step, random numbers $\leq 10^{-6}$ were added to the real and imaginary part of each oscillator to provoke the breakup of potential unstable clusters. Maxima of $\text{Re}(w_k)$ were plotted for the last 2000 time steps of simulation at each c_2 steps.

The schematic in Fig. 3b was drawn based on automatically detected cluster sizes at each c_2 step in the aforementioned c_2 -incremented simulation. These cluster sizes were determined by calculating the pairwise cross-correlations of the trajectories of all oscillators over the last 2000 time steps at each c_2 step, respectively. If the cross-correlation differed from 1 by less than $\epsilon = 10^{-8}$, the two oscillators were deemed to belong to the same cluster. To calculate the cross-correlations and obtain the clusters, we used SciPy's built-in `scipy.cluster.hierarchy.linkage` function.

The schematic in Fig. 3c was determined based on an analogous c_2 -incremented simulations for $N = 32$, $\nu = 0.1$ and $\eta = 0.63$, initialized in the 16-16 configuration at $c_2 = -0.74$. Here, $\Delta c_2 = 2 \cdot 10^{-5}$ and $\Delta T = 10^4$. The simulation was performed until $c_2 = -0.712$, producing the result in Supplementary Figure 1a. Clusters were calculated as in the $N = 16$ case based on the last 800 time steps of simulation at each c_2 step, producing Supplementary Figure 2b.

The schematic in Fig. 3d was determined based on two analogous c_2 -incremented simulations for $N = 256$, $\nu = 0.1$ and $\eta = 0.63$. In the first of these, the ensemble was initialized in the 128-64-64 configuration at $c_2 = -0.7145$, from where c_2 was incremented by $\Delta c_2 = 10^{-5}$ every $\Delta T = 2 \cdot 10^4$ time steps until $c_2 = -0.7117$, producing the result in Supplementary Figure 2a. In a second c_2 -incremented simulation for $N = 256$, the ensemble was initialized at $c_2 = -0.71172$

in the 128-64-33-16-15 configuration found there in the prior $N = 256$ simulation with $\Delta c_2 = 10^{-5}$. From there on, c_2 was incremented by $\Delta c_2 = 2 \cdot 10^{-7}$ every $\Delta T = 2 \cdot 10^4$ time steps until $c_2 = -0.7116$, producing the result in Supplementary Figure 3a-b. For either simulation, clusters were calculated based on the last 800 time steps of simulation at each c_2 step, producing Supplementary Figures 2b and 3b-c, respectively.

Fig. 4b-d were created by simulating the 16-9-(7 × 1) solution in Fig. 4a for $T = 10^6$ time steps. Every 10^4 time steps, the pairwise cross-correlation between all oscillators was calculated over an interval of 800 time steps, and if the cross-correlation of two oscillators was found to be greater than $1 - \epsilon$ for $\epsilon = 10^{-8}$ (Fig. 4b), $\epsilon = 10^{-4}$ (Fig. 4c) or $\epsilon = 10^{-2}$ (Fig. 4d), respectively, they were counted as being in the same cluster.

The solutions in Fig. 5 were obtained by initializing the $N = 20$ ensemble in a 15-5 solution at $c_2 = -0.88$, $\nu = 0.1$ and $\eta = 0.67$, and incrementing c_2 by $\Delta c_2 = 2 \cdot 10^{-4}$ every $\Delta T = 5000$ time steps until $c_2 = -0.7$. Supplementary Figures 4 to 7 were created based on data obtained analogously to that in Figs. 3 and 5 with parameters as given in their respective captions.

DATA AVAILABILITY

Data are available from the authors upon request.

ACKNOWLEDGMENTS

The authors thank Felix P. Kemeth and Maximilian Patzauer for fruitful discussions. Financial support from the Studienstiftung des deutschen Volkes and the Deutsche Forschungsgemeinschaft, project KR1189/18 "Chimera States and Beyond", is gratefully acknowledged.

AUTHOR CONTRIBUTIONS

S.W.H. carried out the simulations and analysed the data. Both authors discussed the results and wrote the paper. K.K. supervised the project.

COMPETING INTERESTS

The authors declare no competing interests.